1

Supplementary Information for

Dynamics and characteristics of dry and moist heatwaves over East Asia

Kyung-Ja Ha[1,2*], Ye-Won Seo[1*], Ji-Hye Yeo[1,2], Axel Timmermann[1,3], Eui-Seok Chung[4*], Christian L. E. Franzke[1,3], Johnny C. L. Chan[5], Sang-Wook Yeh[6], and Mingfang Ting[7]

[1]Center for Climate Physics, Institute for Basic Science, Busan, South Korea

[2]Department of Atmospheric Sciences, Pusan National University, Busan, South Korea

[3]Pusan National University, Busan, South Korea

[4]Korea Polar Research Institute, Incheon, South Korea

[5]School of Energy and Environment, City University of Hong Kong, Hong Kong, China

[6]Department of Marine Science and Convergence Engineering, Hanyang University, Ansan, South Korea

[7]Lamont-Doherty Earth Observatory, Columbia University, Palisades, NY, USA

Supplementary Methods

Heat stress index (HI)

To assess the stress induced by the combined effects of high temperature and humidity, the heat stress index (HI) was calculated by air temperature and relative humidity used by NOAA[1]. The HI is a measure of how hot it really feels when relative humidity is factored in with the actual air temperature. This index was developed through a multiple regression analysis. First, the simple formula applied to calculate the heat index values,

$$\mathrm{HI} = 0.5 \times [\mathrm{T} + 61 + (\mathrm{T} - 68) \times 1.2 + \mathrm{RH} \times 0.094] \quad (1)$$

where T is air temperature in degrees Fahrenheit and RH is relative humidity in percent. If this heat index value is greater than 80, the full regression equation of Rothfusz described below is applied.

$$\begin{aligned} \mathrm{HI} = {} & -42.379 + 2.04901523 \times \mathrm{T} + 10.14333127 \times \mathrm{RH} \\ & - 0.22475541 \times \mathrm{T} \times \mathrm{RH} - 0.00683783 \times \mathrm{T}^2 \\ & - 0.05481717 \times \mathrm{RH}^2 + 0.00122874 \times T^2 \times RH \\ & + 0.00085282 \times T \times RH^2 - 0.00000199 \times T^2 \times RH^2 \end{aligned} \quad (2)$$

If the RH is less than 13% and the T is between 80 ºF and 112 ºF, the following adjustment was subtracted from HI:

$$\mathrm{Adjustment1} = \left(\frac{13 - RH}{4}\right) \times \sqrt{17 - \frac{|T - 95|}{17}} \quad (3)$$

In addition, if RH is greater than 85% and T is between 80 ºF and 87 ºF, the second adjustment is added to HI:

$$\mathrm{Adjustment2} = \left(\frac{RH - 85}{10}\right) \times \left(\frac{87 - T}{5}\right) \quad (4)$$

The HI values were calculated for each day and then we extracted the values of all of the heatwave days. The HI values have 5 ranges corresponding levels of heat stress (i.e., categories); HI =< 80, Safe; 80 – 90, Caution; 90 – 105, Extreme caution; 105 – 130, Danger; >=130, Extreme danger.

Temperature budget equation

In order to explain the physical process contribution to the heatwave onset, the temperature budget equation was analyzed. Temperature change at each pressure level could be written as follows:

$$\frac{\partial \mathbf{T}}{\partial \mathrm{t}} = -\mathbf{V} \cdot \nabla \mathbf{T} + \omega\sigma\frac{p}{R} + \frac{1}{C_p}\frac{d\mathbf{Q}}{dt} \tag{6}$$

where $\mathrm{t}, \mathbf{V}, \nabla, R, p, C_p,$ and $\mathbf{Q}$ represent time, the horizontal velocity vector, the horizontal gradient operator, gas constant, pressure, specific heat at constant pressure, and atmospheric heat source, respectively. Each term denotes temperature tendency, horizontal advection of temperature, adiabatic heating, and diabatic heating. To understand the major contributors to the near-surface heat source, the surface energy budget, which is consist of downward longwave and shortwave radiation flux, upward longwave and shortwave radiation flux, sensible heat flux, and latent heat flux, was considered.

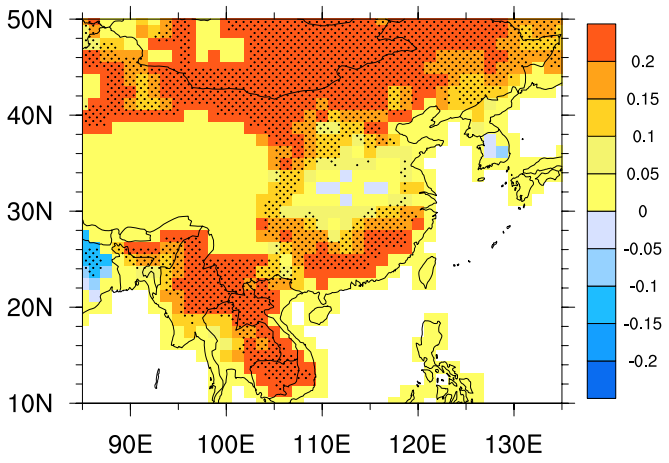

Supplementary Figure 1. The linear trend of heatwave duration. The linear trends of heatwave days [days year^{-1}] based on JRA-55 data from 1958 to 2019. The dots indicate the 90% confidence level using P-value. The hashtags indicate above 2,000m in geopotential height.

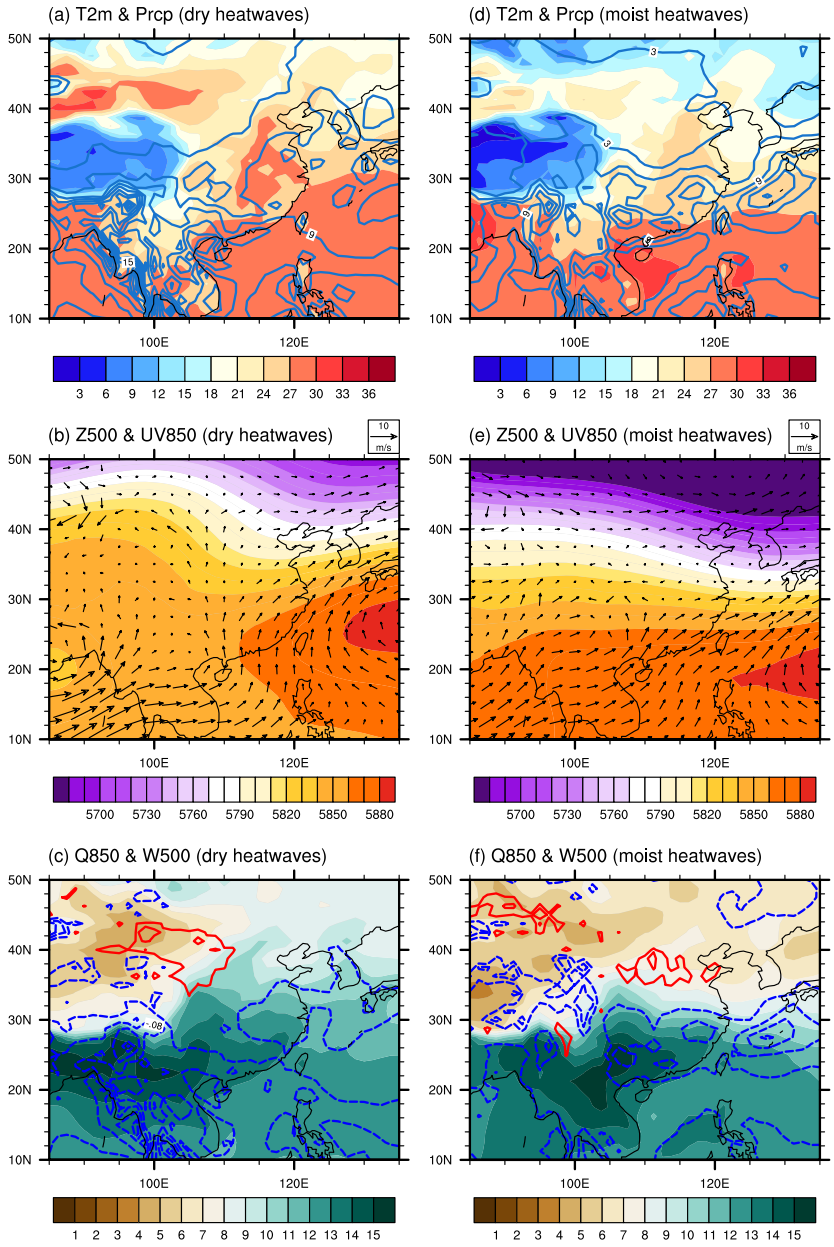

Supplementary Figure 2. Composites for heatwave days over dry and moist heatwave regions. Composites relative to long-term daily mean (climatology) of (a, d) 2-m air temperature (shading) [ºC] and precipitation (contours) [mm day^{-1}], (b, e) geopotential height at 500-hPa (shading) [m] and wind at 850-hPa (vectors) [m s^{-1}], and (c, f) specific humidity at 850-hPa (shading) [g kg^{-1}] and omega at 500-hPa (contours) [Pa s^{-1}] for (a-c) dry heatwave days and (d-f) moist heatwave days. Dry and moist heatwave days were determined as days on which the heatwaves occurred simultaneously in more than 40% of the regions with trend above 0.15 days year^{-1} for dry and moist heatwaves, respectively.

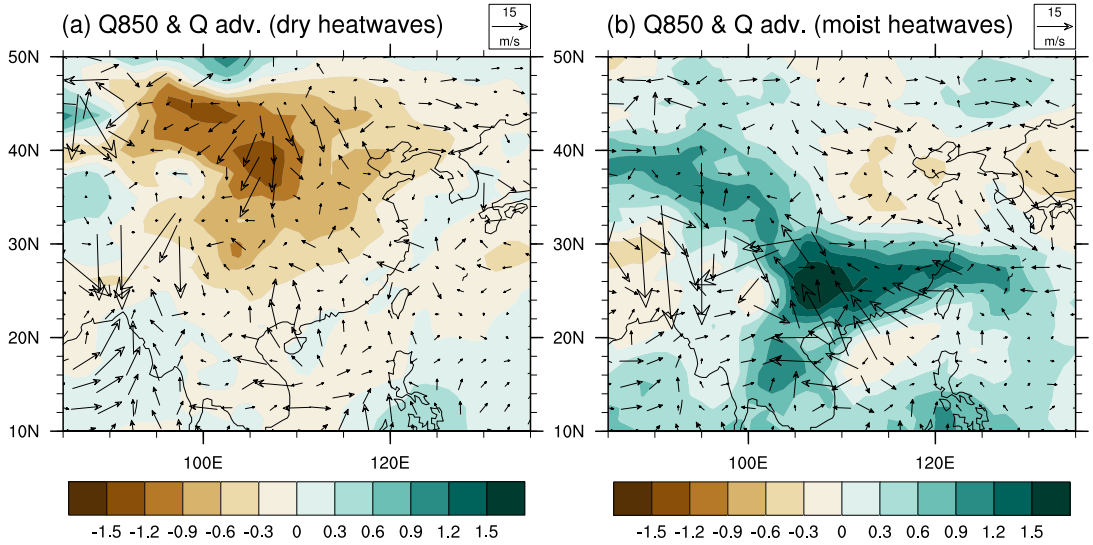

Supplementary Figure 3. Moist Advection and specific humidity for dry and moist heatwave. Anomaly composite of specific humidity at 850-hPa (shading) and composite relative to long-term daily mean (climatology) of moist advection (vectors) at 850-hPa during (a) dry and (b) moist heatwaves.

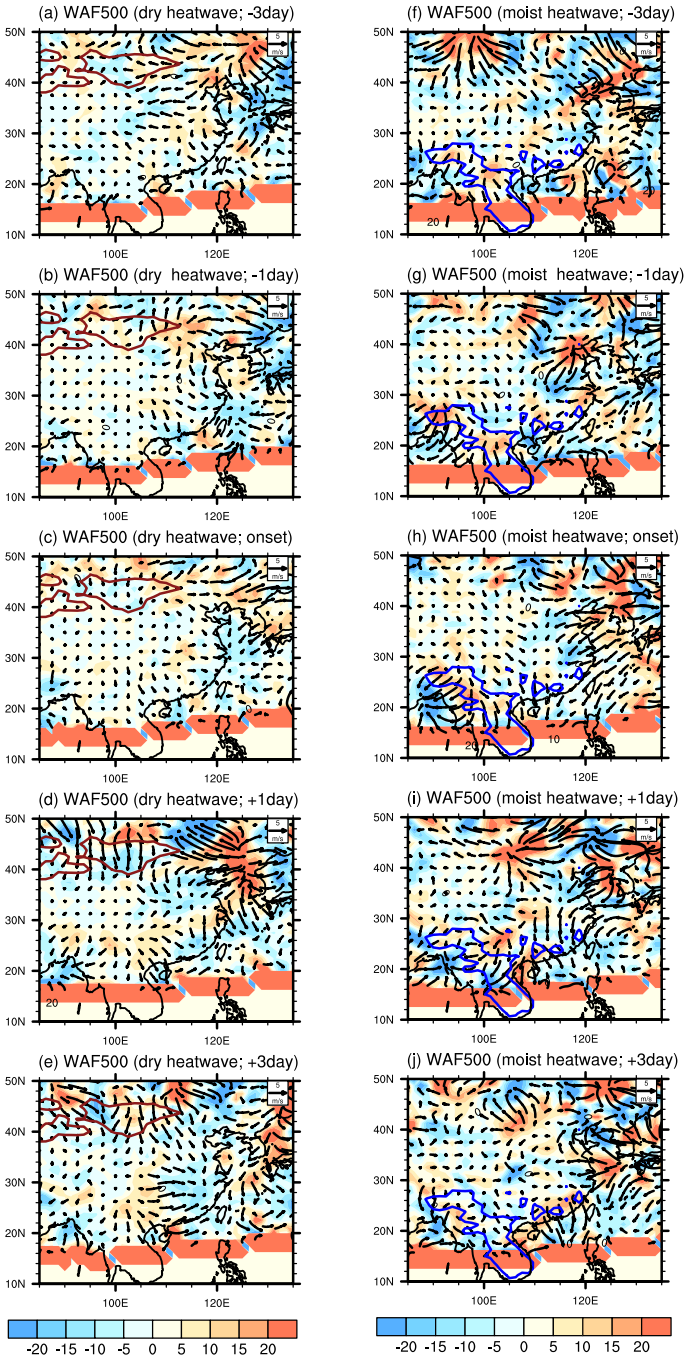

Supplementary Figure 4. Anomalous wave activity flux from 3 days prior to onset up to 3 days after onset of heatwaves. Composite maps of divergence of anomalous wave activity flux (WAF) at 500-hPa (shading) and anomalous WAF at 500-hPa (vectors) before and after the occurrence of (a–e) dry heatwaves and (f–j) moist heatwaves. Red and blue contours represent areas with trend above 0.15 days year^{-1} during 1958–2019 for dry and moist heatwaves, respectively.

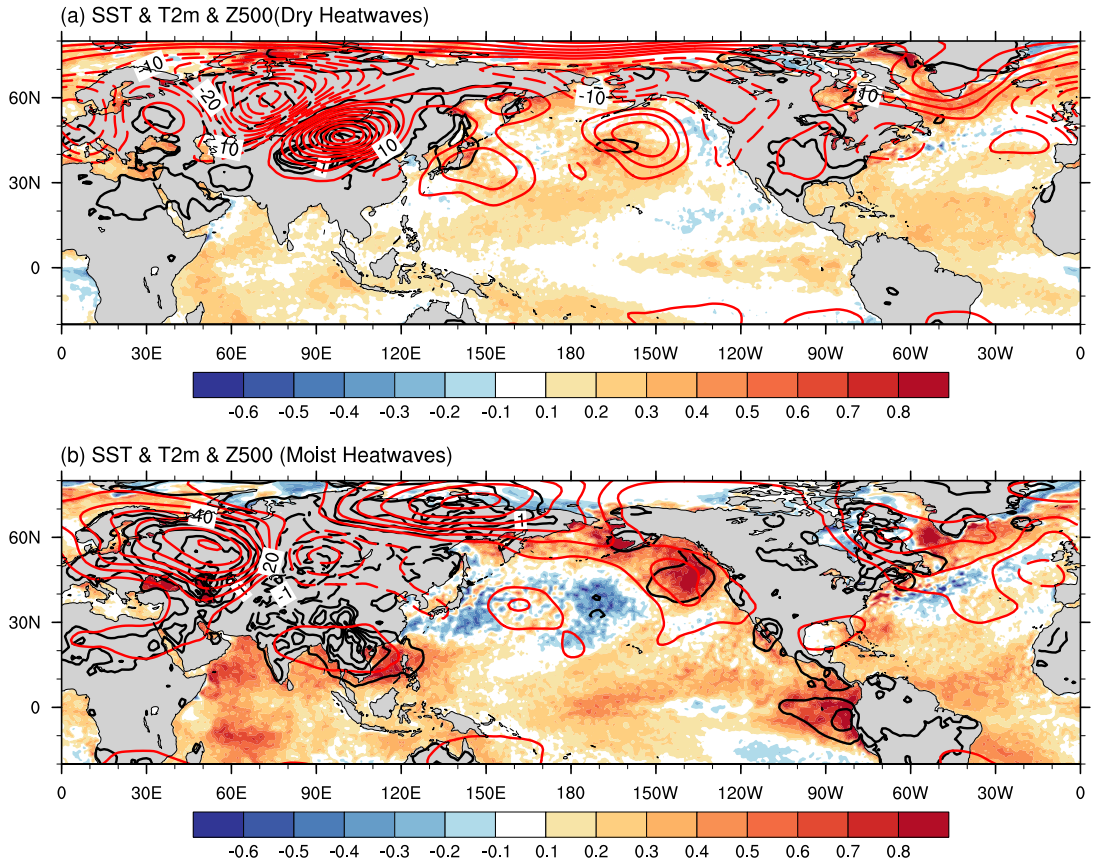

Supplementary Figure 5. Composite of SST, 2-m air temperature, and 500-hPa geopotential height anomalies for heatwave days. Composite of SST, 2-m air temperature, and 500-hPa geopotential height anomalies for heatwave days. Composite of SST (shading), 2-m air temperature (black contour), and 500-hPa geopotential height (red contour) anomalies for all (a) dry and (b) moist heatwave days (normal: daily mean for the period of 1982 to 2019). NOAA OI SST V2 high-resolution dataset was used. 2-m air temperature and geopotential height from JRA-55 were used.

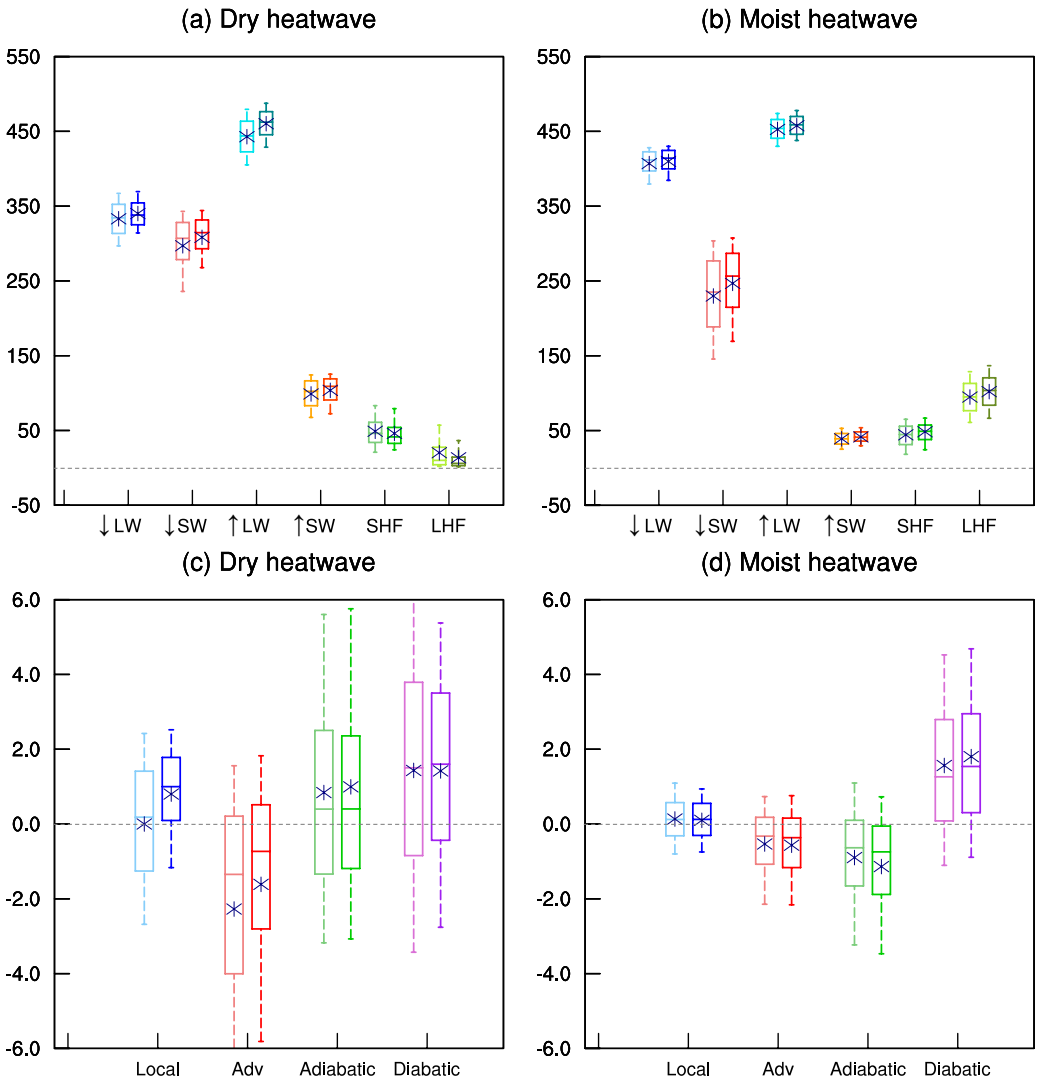

Supplementary Figure 6. Surface energy budget and temperature budget at 975-hPa for dry and moist heatwave days. Surface energy budget (left axis) including downward longwave (↓LW) and shortwave radiation flux (↓SW) [W m^{-2}], upward longwave (↑LW) and shortwave radiation flux (↑SW) [W m^{-2}], surface sensible (SHF) and latent heat flux (LHF) [W m^{-2}] associated with (a) dry heatwaves and (b) moist heatwaves on onset-day (right boxes). Anomalous temperature budget terms at 975-hPa on onset-day (right boxes) associated with (c) dry heatwaves and (d) moist heatwaves [°C day^{-1}]. * denotes the mean value, and the different percentiles depicted in each box are, respectively, the 75th, 50th, and 25th percentile values. The upper and lower lines denote the 90th percentile and the 10th percentile value, respectively.

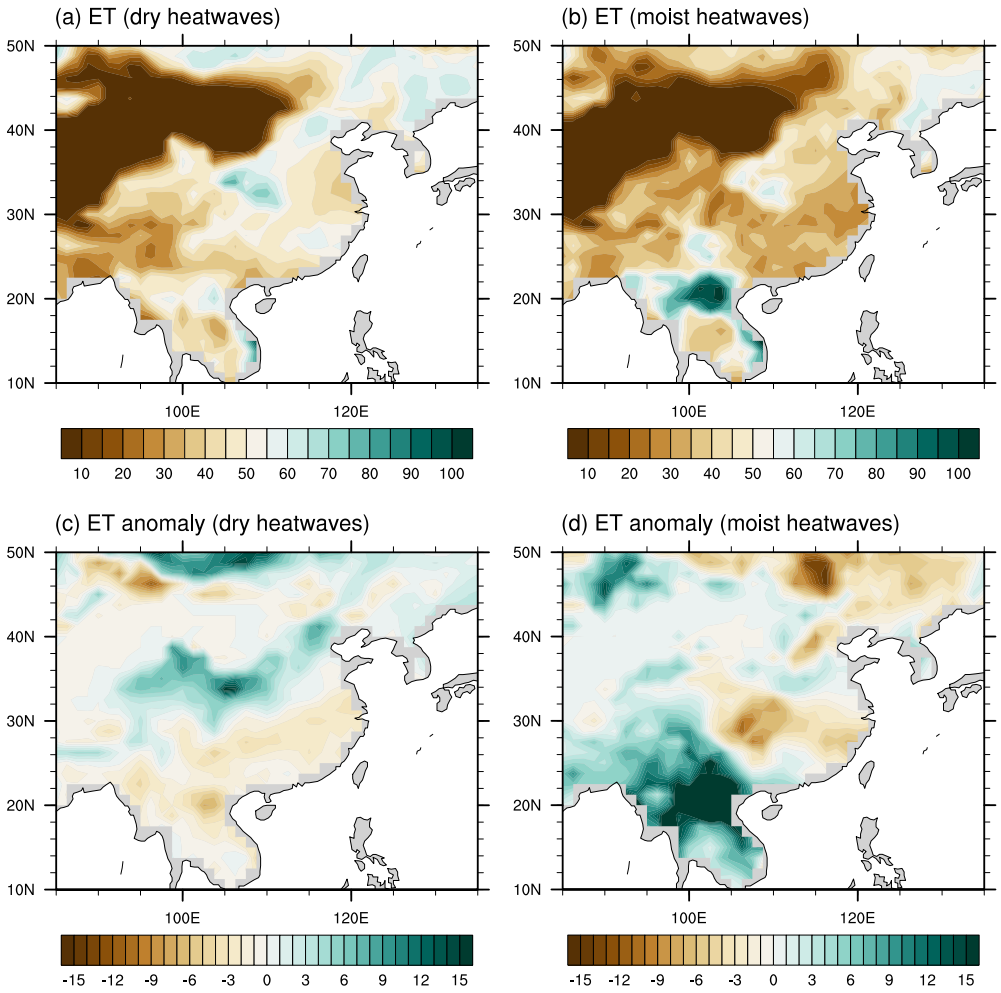

Supplementary Figure 7. Composites of evapotranspiration for heatwave days over dry and moist heatwave regions. (a) Composites and (c) anomaly composites relative to long-term daily mean (climatology) of evapotranspiration (shading) [mm day^{-1}] for dry heatwave days. (b) and (d) are same as (a) and (c), but for moist heatwaves, respectively. Dry and moist heatwave days were determined as days on which the heatwaves occurred simultaneously in more than 40% of the regions with trend above 0.15 days year^{-1} for dry and moist heatwaves, respectively.

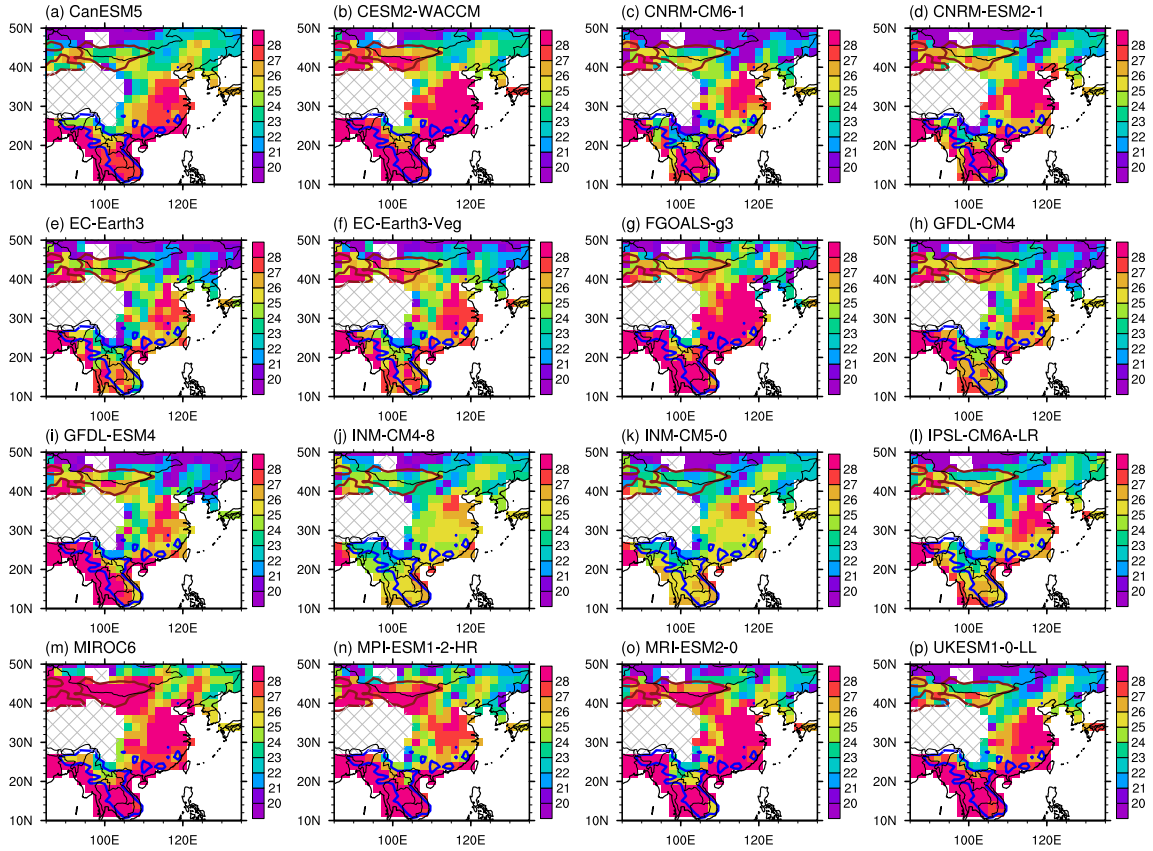

Supplementary Figure 8. The 90th percentile values for daily mean temperature during warm season (MJJASO). The 90th percentile values for daily mean temperature during warm season (MJJASO) in CMIP6 models. Spatial distributions of the 90th percentile values for daily mean temperature during the warm season (MJJASO) over East Asia for the period 1958–2014 from the historical run in CMIP6. The brown and blue contours indicate the area with trend above 0.15 days year^{-1} based on JRA-55 during 1958–2019 for the dry and moist heatwave, respectively. The hashtags indicate above 2,000m in geopotential height.

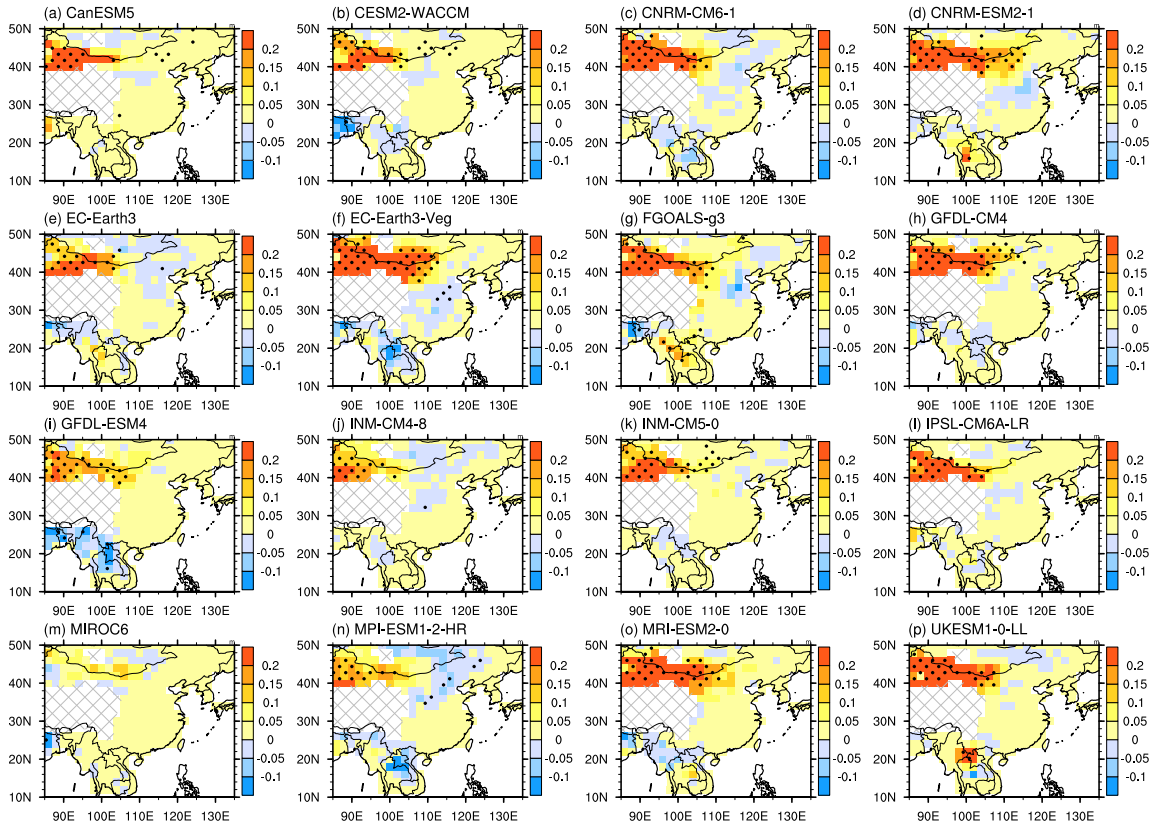

Supplementary Figure 9. The linear trend of dry heatwave duration. The linear trend of dry heatwave duration in CMIP6 models. The linear trends [days year^{-1}] for dry heatwave days during the period from 1958 to 2014 from the historical run of CMIP6. The dots indicate the 90% confidence level using P-value. The hashtags indicate above 2,000m in geopotential height.

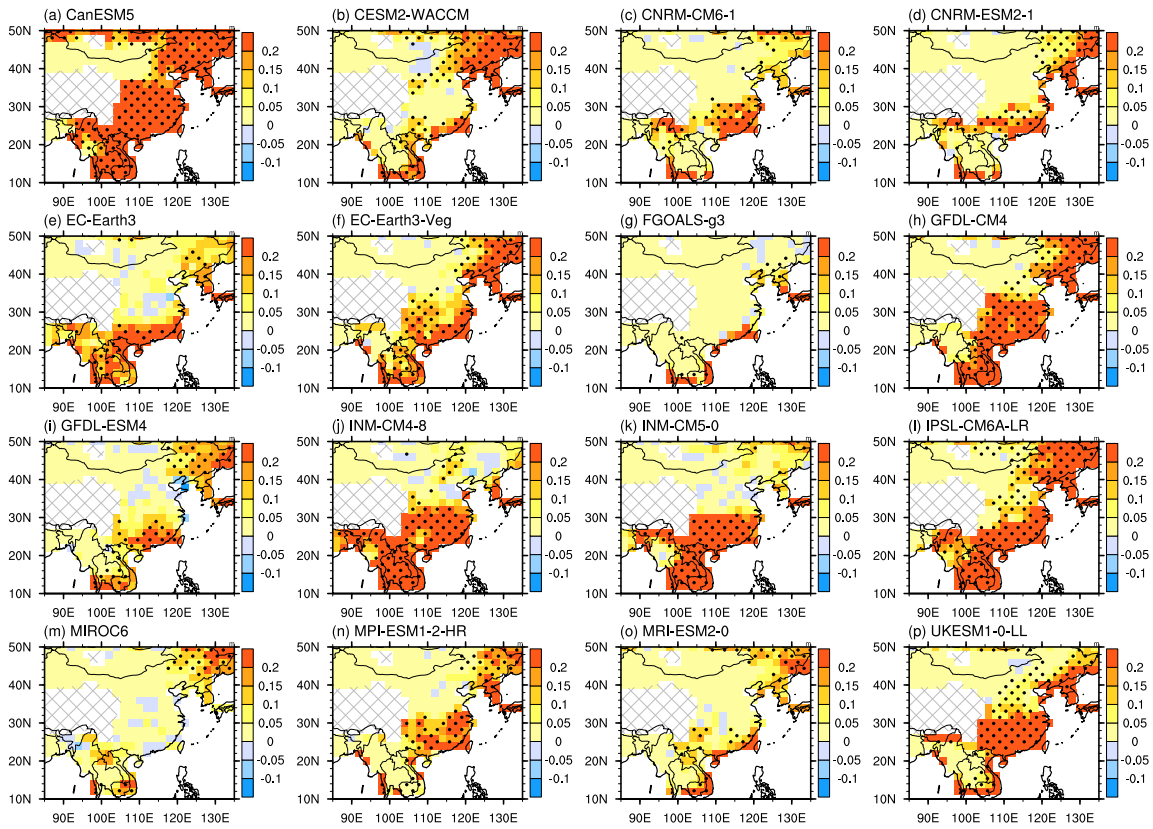

Supplementary Figure 10. The linear trend of moist heatwave duration. The linear trend of moist heatwave duration in CMIP6 models. Same as Supplementary Fig. 9 but for moist heatwaves.

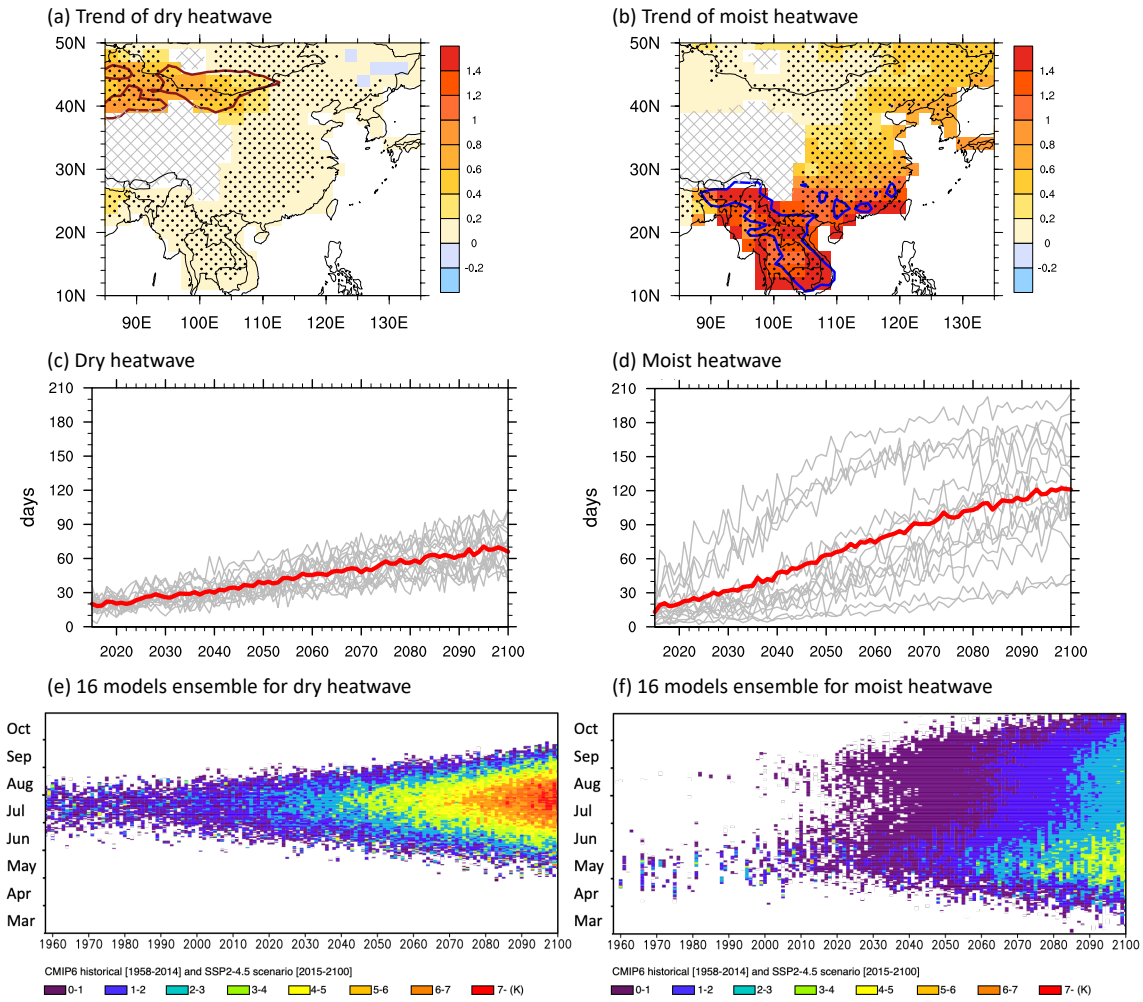

Supplementary Figure 11. Heatwaves over dry and moist heatwave regions during 1958–2014 using JRA-55 and their CMIP6 SSP5-8.5 scenario for period 2015–2100. (a) Trend of number of dry heatwave days per year and (b) moist heatwaves during the period from 2015 to 2100 based on the multi-model mean. Heatwaves were defined as days on which the 90th percentile of daily mean temperature was reached for at least 3-days, based on the historical run simulation of each model from 1958 to 2014. The dots indicate the 90% confidence level using the P-value. The red and blue contours represent areas with trend above 0.15 days year^{-1} based on JRA-55 data during 1958–2019 for dry and moist heatwaves, respectively. The hatched areas indicate above 2,000 m in geopotential height. Time series of heatwave durations over (c) dry and (d) moist heatwave regions (brown contour in (a) and blue contour in (b)). The gray lines denote the results of each model and the red lines indicate the result of the multi-model ensemble mean. The timing of (e) dry

and (f) moist heatwaves from March to October during 1958 to 2014 based on the historical climate simulation and during 2015 to 2100 based on the SSP5-8.5 scenario in the multi-model mean of CMIP6. Data are shown for regions with trend above 0.15 days $year^{-1}$ for dry and moist heatwaves, respectively. The color scale shows the difference between the daily mean temperature and the 90th temperature percentile. For the future projection, we used the 90th temperature percentiles based on the period from 1958 to 2014 from the historical run simulation of each model.

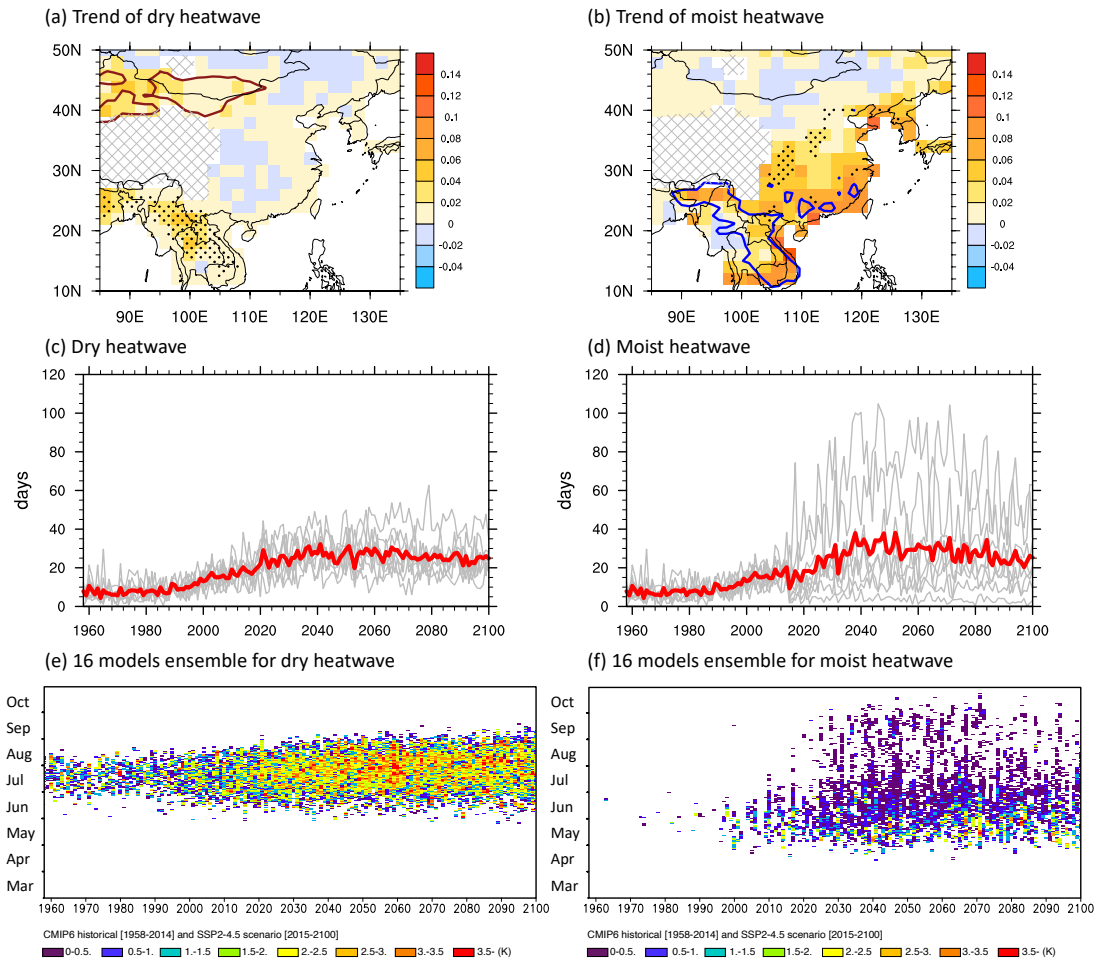

Supplementary Figure 12. Heatwaves over dry and moist heatwave regions during 1958–2014 using JRA-55 and their CMIP6 SSP1-1.9 scenario for period 2015–2100. (a) Trend of number of dry heatwave days per year and (b) moist heatwaves during the period from 2015 to 2100 based on the multi-model mean. Heatwaves were defined as days on which the 90th percentile of daily mean temperature was reached for at least 3-days, based on the historical run simulation of each model from 1958 to 2014. The dots indicate the 90% confidence level using the P-value. The red and blue contours represent areas with trend above 0.15 days year^{-1} based on JRA-55 data during 1958–2019 for dry and moist heatwaves, respectively. The hatched areas indicate above 2,000 m in geopotential height. Time series of heatwave durations over (c) dry and (d) moist heatwave regions (brown contour in (a) and blue contour in (b)). The gray lines denote the results of each model and the red lines indicate the result of the multi-model ensemble mean. The timing of (e) dry and (f) moist heatwaves from March to October during 1958 to 2014 based on the historical

climate simulation and during 2015 to 2100 based on the SSP1-1.9 scenario in the multi-model mean of CMIP6. Data are shown for regions with trend above 0.15 days $year^{-1}$ for dry and moist heatwaves, respectively. The color scale shows the difference between the daily mean temperature and the 90th temperature percentile. For the future projection, we used the 90th temperature percentiles based on the period from 1958 to 2014 from the historical run simulation of each model.

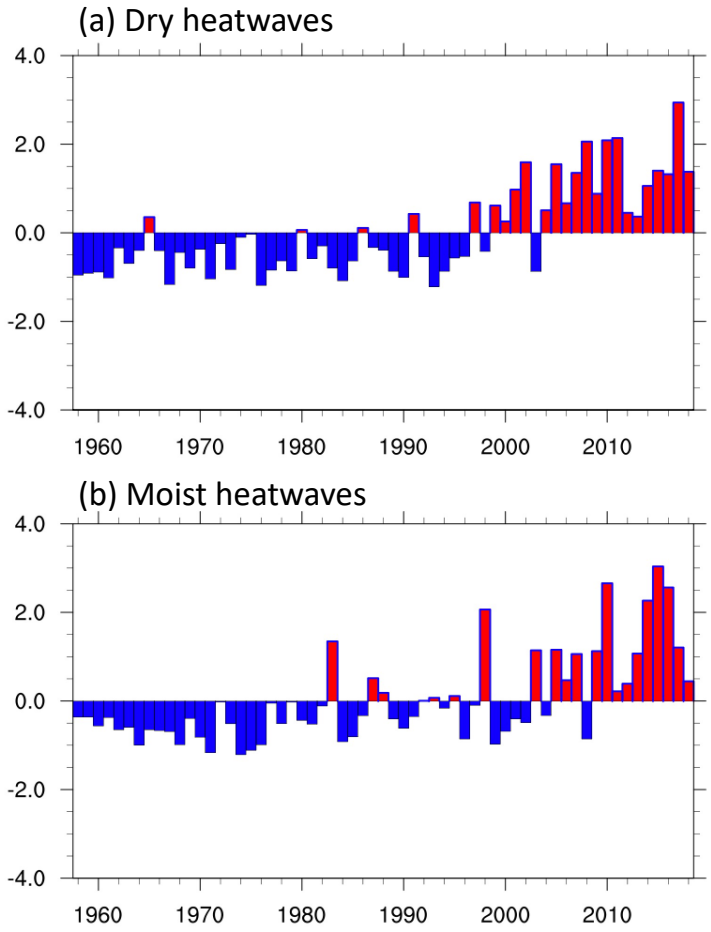

Supplementary Figure 13. Time series of normalized dry and moist heatwave. (a) Time series of normalized (a) dry and (b) moist heatwave durations over dry and moist heatwave regions during 1958–2019, respectively.

Supplementary Table 1. CMIP6 model descriptions. Descriptions of the CMIP6 models used in this study.

Model	Resolution	Source
CanESM5	128 × 64	Canadian Centre for Climate Modelling and Analysis, Canada
CESM2-WACCM	288 × 192	The National Center for Atmospheric Research, USA
CNRM-CM6-1	256 × 128	Centre National de Récherches Météorologiques, France
CNRM-CM5-0		
EC-Earth3	512 × 256	European EC-Earth consortium
EC-Earth3-Veg	512 × 256	
FGOALS-g3	180 × 80	LASG, Institute of Atmospheric Physics, Chinese Academy of Sciences; and CESS, Tsinghua University (LASG-CESS), China
GFDL-CM4	288 × 180	Geophysical Fluid Dynamics Laboratory (GFDL), USA
GFDL-ESM4		
INM-CM4-8	180 × 120	Institute for Numerical Mathematics, Russian Academy of Science, Russia
INM-CM5-0		
IPSL-CM6A-LR	144 × 143	Institute Pierre-Simon Laplace (IPSL), France
MIROC6	256 × 128	Japan Agency for Marine-Earth Science and Technology (JAMSTEC); Atmosphere and Ocean Research Institute (AORI); National Institute for Environmental Studies (NIES); RIKEN Center for Computational Science (R-CCS), Japan
MPI-ESM1-2-HR	384 × 192	Max Planck Institute for Meteorology (MPI), Germany
MRI-ESM2-0	320 × 160	Meteorological Research Institute (MRI)
UKESM1-0-LL	192 × 144	Met Office Hadley Centre (MOHC), UK

Supplementary Reference

1. Rothfusz, L. P. The heat index equation (or, more than you ever wanted to know about heat index). *Tech. Attach. SR/SSD* **90**, 23 (1990).